

Study of the Matrix Effect on the Plasma Characterization of Six Elements in Aluminum Alloys using LIBS With a Portable Echelle Spectrometer

Walid Tawfik Y. Mohamed

*National Inst. of Laser Enhanced Science NILES, Dept. of Environmental Applications, Cairo University, Cairo, Egypt
Faculty of Education for Girls, Department of Physics, Gurayyat, North of Al-gouf, Kingdom of Saudi Arabia*

E-mail: Walid_Tawfik@hotmail.com

Laser-induced breakdown spectroscopy (LIBS) has been applied to perform a study of the matrix effect on the plasma characterization of Fe, Mg, Be, Si, Mn, and Cu in aluminum alloy targets. The generated plasma emissions due to focusing of a 100 mJ Nd: YAG pulsed laser at 1064 nm at the target surface were detected using a portable Echelle spectrometer with intensified CCD camera. Spectroscopic analysis of plasma evolution of laser produced plasmas has been characterized in terms of their spectra, electron density N_e and electron temperature T_e assuming the LTE and optically thin plasma conditions. The obtained average values of T_e and N_e were 7600 K and $3 \times 10^{17} \text{ cm}^{-3}$, respectively, for the six elements in the aluminum alloy samples. The electron density increases with the element concentration while the plasma temperature does not have significance change with concentration. For industrial applications, LIBS with the portable Echelle spectrometer could be applied in the on-line production control that following up elemental concentration in metals and pharmaceuticals by only measuring N_e .

1 Introduction

Laser Induced Plasma Spectroscopy (LIPS or LIBS) is an alternative elemental analysis technology based on the optical emission spectra of the plasma produced by the interaction of high-power laser with gas, solid and liquid media. The increasing popularity of this technique is due to easiness of the experimental set-up and to the wide flexibility in the investigated material that doesn't need any pre-treatment of the sample before the analysis. Obvious tasks for LIBS are certification of metal contents in alloys, trace detection of metals for environmental pollution analysis in soils, on-line control of laser induced industrial processes (e.g. cutting and welding, thin film deposition), quick characterization of material in archaeological objects and works of art, and many others [1–5].

LIBS is based on analysis of line emission from the laser-induced plasma, obtained by focusing a pulsed laser beam onto the sample. The physical and chemical properties of the sample can affect the produced plasma composition, a phenomenon known as the matrix effect. The interaction between the laser and the target in LIBS is influenced significantly by the overall composition of the target, so that the intensity of the emission lines observed is a function of both the concentration of the elements of interest and the properties of the matrix that contains them. Plasma composition is dependent not only on composition of the sample, but also on laser parameters, sample surface conditions as well as on thermal and optical properties of the sample. Previously published works studied the matrix effect under different

experimental conditions to specify causes and find out the methods of correction [6–11]. The different approaches have been undertaken to discriminate the problems resulting from the fractionation of the ablation and matrix effects. The most convenient approach is to determine elemental abundance comparing the analytic line intensities with signals obtained from the proper reference standards having the similar matrix composition. But, it is not always possible to obtain such calibration curves because there are no available standard samples, or it is impossible to have an internal standard of known concentration [12, 13]. In addition, plasma formation dynamics, sample ablation and associated processes are highly non-linear and not fully understood and may also play an important role as reasons of the matrix effect.

Recently an alternative procedure, based on the LIBS technique, for quantitative elemental analysis of solid materials has been proposed, which can, in principle, provide quantitative data with no need of calibration curves or internal standards [14, 15]. The method relies on the assumption about the existence of the stoichiometric ablation and local thermodynamic equilibrium (LTE) i.e. Boltzmann distribution and Saha equation amongst the level population of any species and electron density and temperature of the plasma. However for application of this method experimentally one needs to obtain both equilibrium and thin plasma conditions, a task that may not be always possible to perform. Thus, in spite of the many advantages of LIBS the realization of a quantitative analytical method, which is able to measure main constituents in samples from different matrices, still remains a difficult task because of the complex laser-sample

and laser-plasma interaction mechanisms. As a rule, laser ablation plasma is characterized by complex spatial and temporal structures, and one meets a wide range of varying of parameters during the plasma existence time.

In this paper, we report the optimized conditions for LIBS to analyze the emission spectrum of aluminum alloy samples with high resolution using a portable Echelle spectrometer Mechelle 7500 equipped with ICCD camera. Spectroscopic analysis of plasma evolution of laser produced plasmas has been characterized in terms of their spectra, electron density and electron temperature. The LTE and optically thin plasma conditions were verified for the produced plasma. The electron temperature and density were determined using the emission intensity and stark broadening, respectively, of the spectral lines of six elements Fe, Mg, Be, Si, Mn, and Cu in the aluminum alloys. The dependence of the electron density and temperature on the concentrations of these elements was studied.

2 Experimental setup

2.1 Instrumentation

A typical LIBS experimental setup, described in details by the author elsewhere [6], is used throughout the present investigations. The plasma formation was attained with the aid of a Q-switched Nd: YAG laser (surelite I, continuum, USA) operating at 1064 nm (pulse duration of 7 ns) and repetition rate of 0.1 Hz – 10 Hz. The laser pulse energy of 100 mJ was adjusted by a suitable combination of beam splitters at constant operating high voltage (1.3 kV) and Q-switch delay (1.65 μ s) to ensure spatial and temporal beam profile stability. An energy meter (Nova 978, Ophir Optronics Ltd., USA) was employed to monitor the shot to shot pulse energy. The laser beam was focused on aluminum alloy samples by a 10 cm focal length quartz lens to generate the plasma. A one meter length fused-silica optical fiber (600 μ m diameter) mounted on a micro *xyz*-translation stage is used to collect the emission light from the plasma plume and feed it to a portable Echelle spectrometer of a 0.17 m focal length (Mechelle 7500, Multichannel Instruments, Sweden). The Echelle grating spectrometers designed for operation in high orders and high angles of incidence and diffraction, can provide high resolution in a more compact size and cover a much wider spectral range than conventional grating spectrometers [16]. The Mechelle 7500 provides a constant spectral resolution (CSR) of 7500 corresponding to 4 pixels FWHM over a wavelength range 200–1000 nm displayable in a single spectrum. A gateable, intensified CCD camera, (DiCAM-Pro-12 bit, UV enhanced, 43000 channels, PCO Computer Optics, Germany) coupled to the spectrometer was used for detection of the dispersed light. The overall linear dispersion of the spectrometer camera system ranges from 0.006 (at 200 nm) to 0.033 nm/pixel (at 1000 nm). To avoid the electronic interference and jitters,

the intensifier high voltage was triggered optically. Echelle spectra display, control, processing and analysis were done using both Mechelle software (Multichannel Instruments, Stockholm, Sweden) and GRAMS/32 version 5.1 Spectroscopic Data Analysis Software (Galactic Industries, Salem, NH, USA).

2.2 Optimization of data acquisition procedure

Many optimization procedures were performed to improve our LIBS resolution and sensitivity and to minimize the measurements fluctuations and problems due to the sample heterogeneity.

To improve data reproducibility, and to avoid electronic jittering problem, the laser was set to single shot mode. Then, the Nd:YAG laser beam was focused onto the sample surface at 90° angle. This was done using a 25 mm diameter dichroic mirror that reflects 99% of high energy 1064 nm wavelength. This mirror placed just before the laser-focusing lens as shown in Figure 1. The focal point was set 5 mm below the surface of the sample in order to generate plasma of 800 μ m spot diameter. This also minimize breakdown above the surface of any particles and aerosols generally present above the sample. Moreover, for each new sample, before spectral collection, 20 laser pulses were performed to clean the sample surface and removes surface oxides and contamination to ensure that the observed spectrum is representative of the sample composition. Furthermore, we found that enhancement of the data reproducibility can be achieved by accumulation of consecutive measured spectra for exposures of duration 1000 ns, each delayed 2500 ns from the laser pulse. These values of delay time and exposure window time (gate time) for the ICCD camera produced spectra with minimal background and signals from major lines that did not saturate the detector.

On the other hand, the use of a micro *xyz*-translation stage as a holder for fused-silica optical fiber facilities maximum intensity of the observed emission light from the plasma plume. We investigated a set of eight standard samples of aluminum alloy to study the dependence of the electron density and temperature on the concentrations of six elements Be, Mg, Si, Mn, Fe and Cu by the proposed LIBS setup. So that, these samples, which have never been treated before using LIBS with Mechelle 7500, were selected to have the six elements with a range of concentrations. We used disk shaped standard samples of aluminum alloy provided by Alcan International Limited (0.5 cm; $\phi = 5$ cm). The concentrations of Mg, Si, Be, Cu, Mn and Fe in the aluminum alloy samples are given in Table 1.

Now, we aim to produce LIBS spectra with high precision. Precision is the measure of the degree of reproducibility of a measurement. Laser shot-to-shot variation causes differences in the plasma properties, therefore affects the magnitude of the element signal, and hence degrades the LIBS

Sample	Be	Mg	Si	Fe	Cu	Mn	Al
AL 3104	0.0011	1.15	0.21	0.42	0.17	0.92	Balance
AL 4104	0.0017	1.56	9.63	0.7	0.12	0.046	Balance
AL 5052	0.0043	2.51	0.087	0.33	0.042	0.09	Balance
AL 5182	0.0012	4.67	0.11	0.27	0.061	0.35	Balance
AL 5754	0.0022	2.54	0.22	0.35	0.1	0.29	Balance
AL 6063	0.00030	0.54	0.43	0.2	0.085	0.081	Balance
AL 7010	0.0007	2.44	0.11	0.22	1.88	0.082	Balance
AL a380.2	0.00036	0.028	9.17	0.41	3.61	0.042	Balance

Table 1: Beryllium, copper, iron, magnesium, silicon and manganese concentrations (in w/w %) in the standard aluminum alloy samples.

precision. To improve LIBS precision, spectra from several laser shots have to be averaged in order to reduce statistical error due to laser shot-to-shot fluctuation. We reproduced the measurements at five locations on the sample surface in order to avoid problems linked to sample heterogeneity. Twenty shots were fired at each location and saved in separated files and the average was computed and saved to serve as the library spectrum. For each recorded spectrum, the peak intensity, the Lorentzian curve fitting, the full width at half maximum FWHM, and the center wavelength of each line, as well as the background emission continuum are determined. Data treatment preprocessing of the averaged spectra data was performed in the Windows environment on a Pentium 4 PC using GRAMS/32, Excel (Microsoft Office Excel 2003) and Origin software version 7.0220 (Origin Lab Co., USA). The averages of peak tables (lists of wavelengths and intensities) of the averaged spectra were roll generated in GRAMS/32 and exported for data evaluation.

3 Results and discussion

3.1 LIBS spectrum

Figure 1 shows a typical plasma emission spectrum for aluminum alloy sample AL 7010. This spectrum is the average of 100 single shot spectra recorded at 2.5 μ s delay time and 1 μ s gate width. The panoramic Echelle spectra in the spectral range 200–700 nm show the UV emission lines of aluminum as a major element and the emission lines of Si, Cu, Be, Fe, Mn and Mg in the aluminum alloy sample. Moreover, our observed spectra reflect the wide spectral range and the high resolution of the used spectroscopic system.

3.2 Electron temperature measurements

In LIBS experiments, assuming optically thin plasma and the local thermodynamic equilibrium (LTE) conditions are hold, the re-absorption effects of plasma emission are negligible (i.e. the main ionization process is produced through impact excitation by thermal electrons). Upon these conditions, a Boltzmann population distribution can be assumed in describing the actual thermodynamics parameters of the plas-

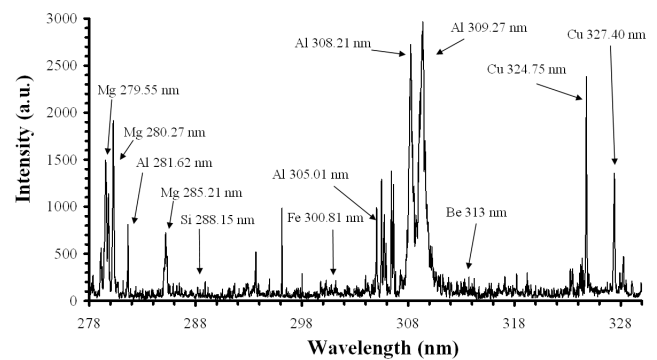


Fig. 1: Typical LIBS spectrum for aluminum alloy sample AL 7010. The laser energy was 100 mJ at wavelength 1064 nm, plasma emissions are accumulated with delay 2.5 μ s, and gate width 1 μ s.

ma. So, the emitted spectral line intensity I is a measure of the population of the corresponding energy level of this element in the plasma. Then I corresponding to the transition between levels E_k and E_i of the atomic species α with concentration C_α , can be expressed as

$$I_\alpha^{ki} = F C_\alpha \frac{g_k A_{ki} e^{-\frac{E_k}{K_B T}}}{U_\alpha(T)}, \quad (1)$$

where K_B is the Boltzmann constant, $U_\alpha(T)$ is the partition function, A_{ki} is the transition probability, g_k is the statistical weight for the upper level, E_k is the excited level energy, T is the temperature (in LTE all temperatures are assumed to be equal, i.e. $T_e \approx T_{ion} \approx T_{plasma}$) and F is a constant depending on experimental conditions.

Equation (1) allows also for evaluating C_α when the sample and reference plasma temperature are different, once the atomic parameters are derived from atomic databases. In order to evaluate the plasma temperature, they take the natural logarithm of Equation (1), obtaining

$$\ln \left(\frac{I_\alpha^{ki}}{g_k A_{ki}} \right) = \frac{E_k}{K_B T} + \ln \left(\frac{C_\alpha F}{U_\alpha(T_\alpha)} \right). \quad (2)$$

In the two-dimensional Boltzmann plane identified by the left hand term of Equation (2) and by E_k , different

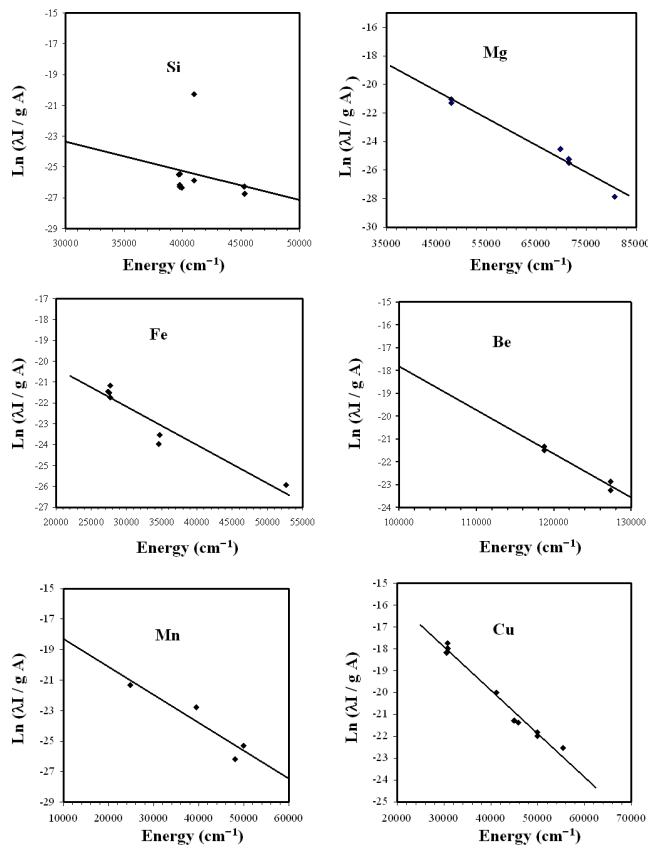


Fig. 2: Six Boltzmann plots were determined from the emission line intensities of Si, Mg, Fe, Be, Mn and Cu observed in the laser-induced plasma of aluminum alloy sample AL 7010. The slope of the plotted curves yields temperatures of 7606 K, 7562 K, 7817 K, 7511 K, 7842 K, and 7224 K for the elements Si, Mg, Fe, Be, Mn, and Cu respectively.

emission lines intensities belonging to the same element in the same spectrum lie along a straight line with a slope of $-1/K_B T$ [21].

In our experiment, the temperatures were determined from the emission line intensities of Mg, Si, Be, Cu, Mn and Fe observed in the laser-induced plasma of aluminum alloys. Figure 2 show six Boltzmann plots of Eqn. (2), for each of these six elements in the aluminum alloy sample AL 7010 where the data were fitted with the least-square approximation. The spectral lines wavelengths, energies of the upper levels, statistical weights, and transition probabilities used for each element are obtained from NIST [17] and Griem [21], and listed in Table 2. The slope of the plotted curves yields temperatures 7606 K, 7562 K, 7817 K, 7511 K, 7842 K, and 7224 K for the elements Si, Mg, Fe, Be, Mn, and Cu respectively. The average value of the plasma temperature is 7600 K which agrees with the value obtained by Sabsabi and Cielo [20] under conditions similar to ours. The difference in the plasma temperature of the six elements may be attributed to the difference in the excitation and ionization

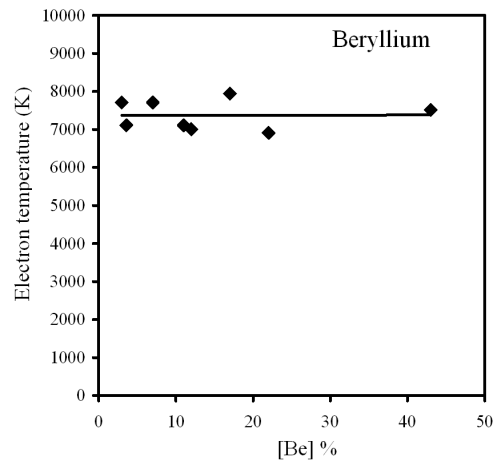


Fig. 3: Electron temperature measured at $2.5 \mu\text{s}$ delay time and $1 \mu\text{s}$ gate width using Boltzmann plot for different concentrations of beryllium in different aluminum alloy samples.

potentials between these elements.

Then the matrix effect on the plasma temperature was studied using the variety of concentrations of the six elements in the eight aluminum samples. This was done by plotting the corresponding temperature for each element versus its concentration in the aluminum alloy samples. Under our experimental conditions, no significance change was found for the plasma temperature with the concentration of the six elements, especially for low concentration elements as shown in Figure 3 as an example for Beryllium. This is could be understanding as follows; for optical thin plasma, increasing the element concentration returns an increasing of the intensity of its corresponding spectral lines with roughly the same ratio, which leads to have the same slope of Boltzmann plot and results in the same plasma temperature.

3.3 Electron density measurements

The usual method for determination of electron density is the measuring of the broadening of a suitable emission line of the laser-plasma spectrum. There are several possible mechanisms of line broadening in plasma: self-absorption, pressure broadening, Doppler broadening, Stark broadening, etc. Lida reported that the line broadening and the spectral shift of the emission line are due mainly to self-absorption phenomenon [18]. In the present study line splitting and the spectral shift, which are good evidence of self-absorption, were monitored carefully. No evidence of line splitting or spectral shift was observed.

Nemet and Kozma reported the broadening of transition lines as pressure, Stark, and Doppler broadening [19]. But pressure and Doppler broadening should not be so much different among transition lines as is the case for plasma of solids. Kyuseok Song *et al.* stated that Stark broadening may be one of the reasons since the broadening effect increases as the energy level increases [22]. Stark broadening results

Element	Wavelength (nm)	A_{ki} (s^{-1})	E_k (cm^{-1})	g_k	Stark broadening parameter w (nm)	Element	Wavelength (nm)	A_{ki} (s^{-1})	E_k (cm^{-1})	g_k	Stark broadening parameter w (nm)
Si	221.89	1.50E+06	45276.18	3	—	Fe	376.01	4.47E+06	45978.00	15	—
Si	243.87	7.40E+05	40991.88	3	—	Fe	376.38	5.44E+07	34547.21	5	—
Si	250.69	4.66E+07	39955.05	5	—	Fe	376.55	9.80E+07	52655.00	15	—
Si	251.43	6.10E+07	39760.28	3	—	Fe	376.72	6.40E+07	34692.14	3	—
Si	251.61	1.21E+08	39955.05	5	—	Fe	378.60	4.20E+06	46026.94	13	—
Si	252.41	1.81E+08	39683.16	1	—	Fe	538.33	5.6E+07	53352.98	13	5.3E-03 [29]
Si	252.85	7.70E+07	39760.28	3	—	Cu	240.00	2.00E+06	67911.85	4	4.1E-3 [21, 28]
Si	288.15	1.89E+08	40991.88	3	0.74E-3 [21]	Cu	261.84	3.07E+07	49382.95	4	—
Si	300.67	1.10E+03	33326.05	5	—	Cu	276.64	9.60E+06	49382.95	4	—
Si	302.00	3.30E+03	33326.05	5	—	Cu	282.44	7.80E+06	46598.34	6	—
Si	390.55	1.18E+07	40991.88	3	1.46E-3 [21]	Cu	296.12	3.76E+06	44963.22	8	—
Mg	277.66	1.32E+08	57873.94	5	—	Cu	306.34	1.55E+06	45879.31	4	—
Mg	277.82	1.82E+08	57833.4	3	—	Cu	319.41	1.55E+06	44544.15	4	—
Mg	277.98	4.09E+08	57873.94	5	—	Cu	324.75	1.39E+08	30783.69	4	—
Mg	278.14	5.43E+08	57812.77	1	—	Cu	327.40	1.37E+08	30535.30	2	—
Mg	278.29	2.14E+08	57833.4	3	—	Cu	333.78	3.80E+05	41153.43	8	—
Mg	279.07	4.01E+08	71491.06	4	—	Cu	402.26	1.90E+07	55387.67	4	—
Mg	279.55	2.60E+08	35760.88	4	—	Cu	406.26	2.10E+07	55391.29	6	—
Mg	279.79	4.79E+08	71490.19	6	—	Cu	427.51	3.45E+07	62403.32	8	—
Mg	280.27	2.57E+08	35669.31	2	—	Cu	465.11	3.80E+07	62403.32	8	—
Mg	281.11	1.96E+08	83520.47	5	—	Cu	510.55	2.00E+06	30783.69	4	—
Mg	281.17	2.11E+08	83511.25	3	—	Cu	515.32	6.00E+07	49935.20	4	—
Mg	285.21	4.91E+08	35051.26	3	3.6E-04 [27]	Cu	521.82	7.50E+07	49942.06	6	—
Mg	291.54	4.09E+08	80693.01	5	—	Cu	529.25	1.09E+07	62403.32	8	—
Mg	292.86	1.15E+08	69804.95	2	—	Cu	570.02	2.40E+05	30783.69	4	—
Mg	293.65	2.30E+08	69804.95	2	—	Cu	578.21	1.65E+06	30535.30	2	—
Fe	370.11	4.80E+07	51192.27	9	—	Mn	258.97	2.6E+08	38543.08	7	5.91E-03 [30]
Fe	370.56	3.22E+06	27394.69	7	—	Mn	401.81	2.54E+07	41932.64	8	—
Fe	371.99	1.62E+07	26874.55	11	—	Mn	403.08	1.70E+07	24802.25	8	—
Fe	372.26	4.97E+06	27559.58	5	—	Mn	403.31	1.65E+07	24788.05	6	—
Fe	372.71	2.00E+07	50534.39	7	—	Mn	403.45	1.58E+07	24779.32	4	—
Fe	373.33	6.20E+06	27666.35	3	—	Mn	404.14	7.87E+07	41789.48	10	—
Fe	373.53	2.40E+07	50475.29	9	—	Mn	404.88	7.50E+07	42143.57	4	—
Fe	373.71	1.42E+07	27166.82	9	—	Mn	405.55	4.31E+07	41932.64	8	—
Fe	373.83	3.80E+07	53093.52	13	—	Mn	405.89	7.25E+07	42198.56	2	—
Fe	374.56	1.15E+07	27394.69	7	—	Mn	406.17	1.90E+07	49415.35	6	—
Fe	374.59	7.33E+06	27666.35	3	—	Mn	406.35	1.69E+07	42053.73	6	—
Fe	374.83	9.15E+06	27559.58	5	—	Mn	407.92	3.80E+07	42143.57	4	—
Fe	375.82	6.34E+07	34328.75	7	—	Mn	408.29	2.95E+07	42053.73	6	—
Mn	408.36	2.80E+07	41932.64	8	—	Be	265.08	1.80E+08	59695.07	3	—
Mn	423.51	9.17E+07	46901.13	6	—	Be	313.04	1.15E+08	31935.32	4	2.81E-05 [21]
Mn	441.49	2.93E+07	45940.93	6	—	Be	313.11	1.15E+08	31928.744	2	—
Mn	445.16	7.98E+07	45754.27	8	—	Be	324.16	1.37E+07	127335.12	2	—
Mn	446.20	7.00E+07	47207.28	10	—	Be	324.18	2.73E+07	127335.12	2	—
Mn	475.40	3.03E+07	39431.31	8	—	Be	327.46	1.43E+07	118761.32	4	—
Mn	478.34	4.01E+07	39431.31	8	—	Be	327.47	1.43E+07	118760.51	2	—
Mn	482.35	4.99E+07	39431.31	8	—	Be	332.10	6.90E+06	52080.94	3	—
Be	265.05	1.08E+08	59697.08	5	—	Be	332.11	2.10E+07	52080.94	3	—
Be	265.06	1.44E+08	59695.07	3	—	Be	332.13	3.40E+07	52080.94	3	—

Table 2: A list of the spectroscopic data of the spectral lines used for the determination of plasma temperature and density of aluminum alloy samples.

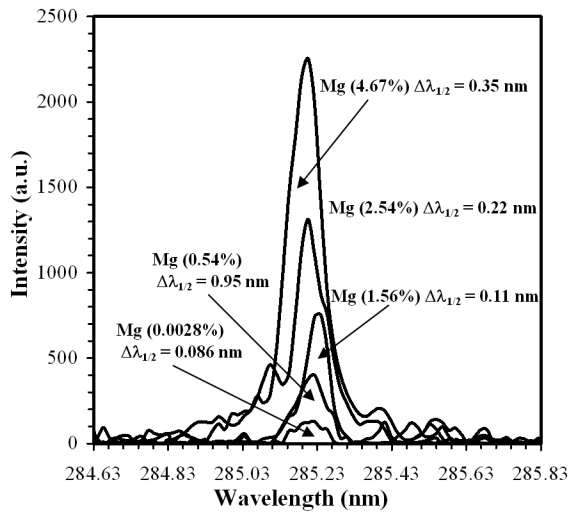


Fig. 4: The 285.21 nm line with sufficient resolution to measure the full width at half-maximum ($\lambda_{1/2}$) at different concentrations of Mg in the aluminum alloys. For each line, the data points were fitted with Lorentzian fitting function using the Origin software to determine ($\lambda_{1/2}$).

from Coulomb interactions between the radiator and the charged particles present in the plasma. Both ions and electrons induce Stark broadening, but electrons are responsible for the major part because of their higher relative velocities. Therefore, in our conditions, the profile of a line is mainly contributed to linewidths arises from the Stark effect while the contribution of other mechanisms of broadening (Doppler effect, Van der Waals broadening, and resonance broadening) can be neglected, as shown under conditions similar to ours by Sabsabi and Cielo [20].

The electrons in the plasma can perturb the energy levels of the individual ions which broaden the emission lines originating from these excited levels. Stark broadening of well-isolated lines in the plasma is, thus, useful for estimating the electron number densities provided that the Stark-broadening coefficients have been measured or calculated. The line profile for stark broadened is well described by a Lorentzian function

Since the instrumental line-broadening exhibit Gaussian shape, then the stark line width $\Delta\lambda_{FWHM}$ can be extracted from the measured line width $\Delta\lambda_{observed}$ by subtracting the instrumental line broadening $\Delta\lambda_{instrument}$:

$$\Delta\lambda_{FWHM} = \Delta\lambda_{observed} - \Delta\lambda_{instrument} . \quad (3)$$

In our case $\Delta\lambda_{instrument}$ was 0.05 nm (determined by measuring the FWHM of the Hg lines emitted by a standard low pressure Hg lamp).

The width of stark broadening spectral line depends on the electron density N_e . Both the linear and the quadratic stark effect are encountered in spectroscopy. Only the hydrogen atom and H-like ion exhibit the linear stark effect. For the linear stark effect the electron density should be deduced

from H line width from the formula [21]

$$N_e = C(N_e, T) \Delta\lambda_{FWHM}^{3/2} \quad (4)$$

the values of the parameter $C(N_e, T)$ are tabulated in the literature [21], which determine the relative contribution of the electron collision on the electrostatic fields, and depend weakly on N_e and T .

For a non-H-like line, the electron density (in cm^{-3}) could be determined from the FWHM of the line from the formula [21]:

$$N_e \approx \left(\frac{\Delta\lambda_{FWHM}}{2w} \right) \times 10^{16}, \quad (5)$$

where w is the electron impact parameter (stark broadening value) and it is given in Table 2. The last formula is generally used for calculations of plasma generated from solid targets [7, 8, 20].

Six lines were identified as candidates for electron-density measurements: 390.55 nm, 285.21 nm, 538.33 nm, 240.00 nm, 258.97 nm and 313.04 nm for Si, Mg, Fe, Cu, Mn and Be respectively. Figure 4 shows, as an example for Mg, the 285.21 nm line with sufficient resolution to measure the full width at half-maximum ($\lambda_{1/2}$) at different concentrations of Mg in the aluminum alloys. All the six lines data points were fitted with Lorentzian fitting function using the Origin software to determine ($\lambda_{1/2}$) as shown in Fig. 4 for Mg as an example. Substituting the values of $\lambda_{1/2}$ in Eqn. (3) and the corresponding values of stark broadening w from Table 2 in Eqn. (6) the electron density for Mg was determined. These steps were repeated for each concentration of the six elements in the eight aluminum alloy samples. Then the obtained electron density values were plotted versus the element concentration. Figure 5 shows six plots for the variation of the electron density values versus the concentrations of Mg, Si, Be, Fe, Cu and Mn in different aluminum alloy samples. These plots reveal that, in case of Mg, Si, Fe, Cu and Mn, electron density increases with the element concentration. For the case of low concentration elements like Be, the increase of the electron density with the element concentration is very weak. This result might occur because increasing the “element” concentration comprises increasing portion of the laser-target interaction volume which agrees with O. Samek [24] and Rusak *et al.* [25].

Finally, by knowing the electron density and the plasma temperature we can determine whether the local thermodynamic equilibrium (LTE) assumption is valid applying the criterion given by McWhirter [26].

The lower limit for electron density for which the plasma will be in LTE is:

$$N_e \geq 1.4 \times 10^{14} \Delta E^3 T^{1/2}, \quad (6)$$

where ΔE is the largest energy transition for which the condition holds and T is the plasma temperature [23].

In the present case $\Delta E = 3.65$ eV for Al (see Ref. [20])

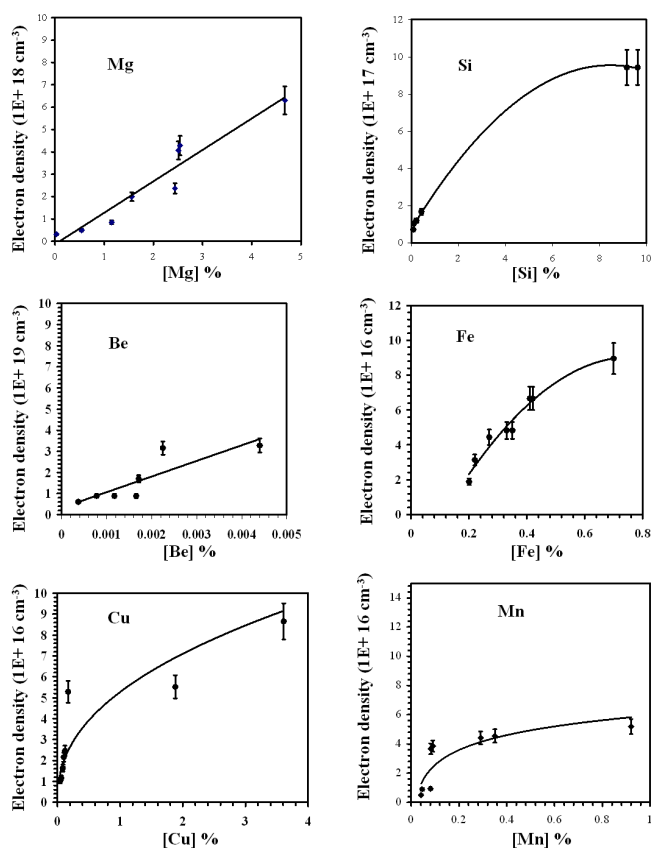


Fig. 5: Six plots for the variation of the electron density values versus the concentrations of Mg, Si, Be, Fe, Cu and Mn in different aluminum alloy samples.

and the electron density lower limit value given by Eqn. (7) is $6 \times 10^{15} \text{ cm}^{-3}$. The experimentally calculated densities are greater than this value, which is consistent with the assumption that the LTE prevailing in the plasma.

4 Conclusion

In summary, we have carried out an accurate LIBS setup using portable commercial Echelle spectrometer equipped with ICCD detector to study aluminum alloys matrix effects on the plasma characterization. The electron density and plasma temperature were determined for six elements (Fe, Mg, Be, Si, Mn, and Cu) in the aluminum alloy targets. The electron density increases with the element concentration while the plasma temperature does not have significance change with the element concentration.

For a plasma diagnostics perspective, the target physical properties play an important role in the obtained values of the laser induced plasma temperature T_e and electron density N_e . For industrial application, LIBS could be applied in the on-line industrial process that following up elemental concentration in metals and pharmaceuticals by only measuring N_e of that element.

Acknowledgment

The author gratefully acknowledges the support of Prof. M. Sabsabi and Prof. M. Abdel-Harith specially for offering the standard aluminum alloy samples.

Submitted on January 20, 2007

Accepted on February 02, 2007

References

1. Radziemski L. J. Review of selected analytical applications of laser plasmas and laser ablation, 1987–1994. *Microchem. J.*, 1994, v. 50, 218–234.
2. Rusak D. A., Castle B. C., Smith B. W. and Winefordner J. D. Fundamentals and applications of laser-induced breakdown spectroscopy. *Crit. Rev. Anal. Chem.*, 1997, v. 27, 257–290.
3. Sneddon J. and Lee Y. Novel and recent applications of elemental determination by laser-induced breakdown spectroscopy. *Anal. Lett.*, 1999, v. 32, 2143–2162.
4. Tognoni E., Palleschi V., Corsi M. and Cristoforetti G. Quantitative micro-analysis by laser-induced breakdown spectroscopy: a review of the experimental approaches. *Spectrochim. Acta Part B*, 2002, v. 57, 1115–1130.
5. Majidi V. and Joseph M. R. Spectroscopic applications of laser-induced plasmas. *Crit. Rev. Anal. Chem.*, 1992, v. 23, 143–162.
6. Bulatov V., Krasniker R. and Schechter I. Study of matrix effects in laser plasma spectroscopy by combined multifiber spatial and temporal resolutions. *Anal. Chem.*, 1998, v. 70, 5302–5310.
7. Sabsabi M., Detalle V., Harith M. A., Walid Tawfik and Imam H. Comparative study of two new commercial Echelle spectrometers equipped with intensified CCD for analysis of laser-induced breakdown spectroscopy. *Applied Optics*, 2003, v. 42, No. 30, 6094–6098.
8. Ismail M. A., Imam H., Elhassan A., Walid Tawfik and Harith M. A. LIBS limit of detection and plasma parameters of some elements in two different metallic matrices. *J. Anal. At. Spectrom.*, 2004, v. 19, 1–7.
9. Xu L., Bulatov V., Gridin V. and Schechter I. Absolute analysis of particulate materials by laser-induced breakdown spectroscopy. *Anal. Chem.*, 1997, v. 69, 2103–2108.
10. Goode S. R., Morgan S. L., Hoskins R. and Oxsher A. Identifying alloys by laser-induced breakdown spectroscopy with a time-resolved high resolution echelle spectrometer. *J. Anal. At. Spectrom.*, 2000, v. 15, 1133–1138.
11. Eppler A. S., Cremers D. A., Hickmott D. D., Ferris M. J. and Koskelo A. C. Matrix effects in the detection of Pb and Ba in soils using laser-induced breakdown spectroscopy. *Appl. Spectrosc.*, 1996, v. 50, 1175–1181.
12. Quentmeier A., Sdorra W. and Niemax K. Internal standardization in laser induced fluorescence spectrometry of microplasmas produced by laser ablation of solid samples. *Spectrochimica Acta B*, 1990, v. 45, No. 6, 5371–5379.

13. Bassiottis I., Diamantopoulou A., Giannoundakos A., Roubani-Kalantzopoulou F. and Kompitsas M. Effects of experimental parameters in quantitative analysis of steel alloy by laser-induced breakdown spectroscopy. *Spectrochim. Acta Part B*, 2001, v. 56, 671–683.
14. Ciucci A., Corsi M., Palleschi V., Rastelli V., Salvetti A. and Tognoni E. A new procedure for quantitative elemental analyses by laser induced plasma spectroscopy. *Applied Spectroscopy*, 1999, v. 53, 960–964.
15. Bulajic D., Corsi M., Cristoforetti G., Legnaioli S., Palleschi V., Solveti A. and Rognoni E. A procedure for correcting self-absorption in calibration-free laser induced breakdown spectroscopy. *Spectrochim. Acta B*, 2002, v. 57, 339–353.
16. Corsi M., Palleschi V., Salvetti A. and Tognoni T. Making LIBS quantitative: a critical review of the current approaches to the problem. *Res. Adv. Appl. Spectrosc.*, 2000, v. 1, 41–47.
17. Olesik J.W. Echelle grating spectrometers for inductively coupled plasma-optical emission spectrometry. *Spectroscopy*, 1999, v. 14, No. 10, 27–30.
18. NIST National Institute of Standards and Technology, USA, electronic database, http://physics.nist.gov/PhysRefData/ASD/lines_form.html
19. Lida Y. Effects of atmosphere on laser vaporization and excitation processes of solid samples. *Spectrochim. Acta B*, 1990, v. 45, 1353–1367.
20. Nemet B. and Kozma L. Time-resolved optical emission spectrometry of Q-switched Nd:YAG laser-induced plasmas from copper targets in air at atmospheric pressure. *Spectrochim. Acta B*, 1995, v. 50, 1869–1888.
21. Sabsabi M. and Cielo P. Quantitative analysis of aluminum alloys by laser-induced breakdown spectroscopy and plasma characterization. *Applied Spectroscopy*, 1995, v. 49, No. 4, 499–507.
22. Griem H.R. Plasma spectroscopy. McGraw-Hill, New York, 1964.
23. Kyuseok Song, Hyunki Cha, Jongmin Lee and Yong Lee. Investigation of the line-broadening mechanism for laser-induced copper plasma by time-resolved laser-induced breakdown spectroscopy. *Microchem. Journal*, 1999, v. 63, 53–60.
24. Bekefi G. Principles of laser plasmas. Wiley, New York, 1976, 550–605.
25. Samek O., Beddows D.C.S., Telle H.H., Kaiser J., Liska M., Caceres J.O. and Gonzales Urena A. Quantitative laser-induced breakdown spectroscopy analysis of calcified tissue samples. *Spectrochimica Acta Part B*, 2001, v. 56, 865–875.
26. Rusak D.A., Clara M., Austin E.E., Visser K., Niessner R., Smith B.W. and Winefordner J.D. Investigation of the effect of target water content on a laser-induced plasma. *Applied Spectroscopy*, 1997, v. 51, No. 11, 1628–1631.
27. McWhirter R.W.P. In: *Plasma Diagnostic Techniques*, ed. R.H. Huddleston and S.L. Leonard, Academic Press, New York, 1965, Ch. 5, 206.
28. Le Drogoff B., Margotb J., Chakera M., Sabsabi M., Barthelemy O., Johnstona T.W., Lavillea S., Vidala F. and von Kaenela Y. Temporal characterization of femtosecond laser pulses induced plasma for spectrochemical analysis of aluminum alloys. *Spectrochimica Acta Part B*, 2001, v. 56, 987–1002.
29. Konjevic N. and Wiese W.L. Stark widths and shifts for spectral lines of neutral and ionized atoms. *J. Phys. Chem. Ref. Data*, 1990, v. 19, 1337.
30. Freudestien S. and Cooper J. Stark broadening of Fe I 5383 Å. *Astron. & Astrophys.*, 1979, v. 71, 283–288.
31. Popovic L.C. and Dimitrijevic M. S. Tables of the electron impact broadening parameters: Mn II, Mn III, Ga III, Ge III and Ge IV Lines. *Bull. Astron. Belgrade*, 1997, No. 156, 173–178.